Solar and Stellar Flares and their Effects on Planets
Proceedings IAU Symposium No. 320, 2015
A.G. Kosovichev, S.L. Hawley & P. Heinzel, eds.

doi:10.1017/S1743921316002155

Characterization of X-ray flare properties of AB Dor

S. Lalitha[1,2]

[1]Indian Institute of Astrophysics, II Block, Koramangala, Bangalore 560034, India

[2]Tata Institute of Fundamental Research, Homi Bhabha Road, Mumbai 400005, India
email: lalitha.sairam@iiap.res.in

Abstract. The strong similarities between the flares observed on the Sun and in low mass stars has raised question regarding dynamo in these stars. Using the Sun as a prototype, one may be able to address this. In this paper, we present an analysis of 30 intense X-ray flares observed from AB Dor. These flares detected in XMM-Newton data show a rapid rise (500-3000 s) and a slow decay (1000-6000 s). Our studies suggest that the scaling law between the flare peak emission measure and the flare peak temperature for all the flares observed on AB Dor is very similar to the relationship followed by solar flares. Furthermore, we obtain the frequency distribution of flare energies which is a crucial diagnostic to calculate the overall energy residing in a flare. Our results of this study indicate that the large flare ($10^{33} \leqslant E \leqslant 10^{34}$ erg) may not contribute to the heating of the corona.

Keywords. Sun: activity, stars: flare, stars: coronae, stars: individual: AB Dor, X-rays: stars

1. Introduction

Nearly 70% of the stars in our galaxy comprise of low mass stars making them the most common stars in the solar neighbourhood, in-turn making them the most frequent planet hosts Henry *et al.* 2004. Active low mass stars also known as flare stars, are strong coronal X-ray sources. Low mass stars posses a largely neutral photosphere and a cool effective temperature in camparison to the Sun, however, they have a strong magnetic dynamos. These stars transfer energy from magnetic field into the outer atmospheres by non-radiative heating process, which powers the steady-state emission as well as energetic flares affecting the orbiting planets. Such magnetic activity/heating has been observed in stars for decades across the electromagnetic spectrum. However, the exact mechanism that controls the acitivity in active low-mass stars are still not well understood. Since low mass stars are capable of producing strong flares of short as well as longer durations and are also the most numerous of potential planetary hosts, it is essential to understand how frequently and powerfully these stars flare.

AB Dor is a young active K dwarf ($\sim$ 40-50 Myr, Guirado *et al.* 2011). AB Dor is an ultra-fast rotator with a rotational velocity v*sini*90 km/s and a rotation period of 0.514 days Kuerster *et al.* 1994. The rapid rotation results in very high levels of magnetic activity with an average $\log(\frac{L_x}{L_{bol}})\approx$- 3.

AB Dor is a quadruple system consisting of the components AB Dor A, AB Dor Ba, AB Dor Bb and AB Dor C. Located 9.5″ away from AB Dor A is an active M dwarf AB Dor B (Rst 137B; Vilhu & Linsky 1987), about $\sim$60 times bolometrically fainter than AB Dor A, and thus only little or no contamination due to the presence of AB Dor B is expected in data that leave both components unresolved. At radio wavelengths AB Dor B was serendipitously detected with the Australian Telescope Compact Array (ATCA)

during an observation of AB Dor A. However, the binarity of AB Dor B itself with a separation of only 0.7″ (called as AB Dor Ba and AB Dor Bb) was detected only after the advent of adaptive optics. Yet another low mass companion to AB Dor A is AB Dor C, located about 0.16″ away from AB Dor A. For further detailed overview on the companions of AB Dor system see Guirado *et al.* (2011).

Being located as a foreground star of the large magellanic cloud, AB Dor has an advantage of being observed at all times by most of the X-ray satellites. AB Dor is a calibration source for reflection grating spectrometer onboard *XMM-Newton*, hence has been repeatedly observed. During these calibration observations several flares on AB Dor have been recorded providing an ideal opportunity to characterize each of these flares and compare its properties to that of solar flares. Such X-ray flare studies on AB Dor has been carried out by (Lalitha *et al.* 2013a; Lalitha *et al.* 2013b).

In Sect. 2 we describe the observations and the methods used for data analysis. In Sect. 3 we present the results followed by a summary in Sect. 4.

2. Observations and data analysis

AB Dor was observed using *XMM-Newton* using varying detector setups and exposure times. A detailed description of the observations are provided in columns 1 - 4 of Table 1. Useful data were obtained by focussing the X-rays onto the European Imaging Camera (EPIC). XMM-Newton consists of three EPIC cameras - one PN and two MOS cameras with a sensitivity range of ≈0.3-12 keV. The X-ray telescope equipped with the two MOS cameras are also equipped with reflection gratings (RGS). RGS produce high resolution X-ray spectra between 0.35 - 2.5 keV. Useful data of AB Dor were obtained with the EPIC and the RGS detectors, which were operated simultaneously. The data were reduced using standard XMM-Newton Science Analysis System (SAS) software, version 14.0. Spectral analysis were done using *Xspec* version 12.9.0 (Arnaud 1996). We used the multi-component *Xspec* models coupled with abundances. We calculated the abundance relative to the solar photospheric values as given by Grevesse & Sauval (1998). AB Dor is located at a distance of just 15 pc, hence due to the proximity of AB Dor, interstellar absorption is negligible.

We analysed the brightest X-ray flares observed on AB Dor using XMM-Newton observations. We defined an event as a flare when there is an anomaly in the count rate. For example, when the peak count rate increases by 50 or more in comparison to the pre-flare/quiescent level. This results in over 17 PN flares and 28 RGS flares over the last decade. The difference in the number of flares detected by the PN and the RGS is because AB Dor is a calibration source for the RGS and has been observed for longer period when compared to the PN.

We divided each of the flare light curves into smaller time bins and created a spectrum for each of these bins. Analysing these spectra helps in understanding the characteristic evolution of the flare emission measure (EM), temperatures (T) and also provides an insight into the flare loop morphology. Each of the spectra is fitted with combinations of APEC models. A quiescent spectra was generated before and after the flare for each of the observation and fitted with two-temperature component APEC models. The abundance of carbon, nitrogen, oxygen, neon and iron abundances were allowed to vary freely and independently, but were fixed among all temperature components. We note that the properties of the for different quiescent spectra are very similar. Hence we created an average quiescent emission i.e. temperatures ($kT_1 = 0.29 \pm 0.04$ keV, $kT_2 = 0.69 \pm 0.08$ keV and $kT_3 = 2.29 \pm 0.15$ keV) and emission measures ($EM_1 = 1.48 \pm 0.17 \times 10^{52}\ cm^{-3}$, $EM_2 = 4.98 \pm 0.26 \times 10^{52}\ cm^{-3}$ and $EM_3 = 2.18 \pm 0.19 \times 10^{52}\ cm^{-3}$). While the

https://doi.org/10.1017/S1743921316002155 Published online by Cambridge University Press

Table 1. Observation log of *XMM-Newton* data used for analysis. Column 4, 5 and 6 provides the peak flare count rate, peak X-ray flux and X-ray luminosity. In column 7 we list the total integrated flare energy.

Obs. ID	Instrument	Date	Obs. time [ks]	Peak count rate [cts/s]	Peak Flux $\times 10^{-11}$ [erg cm^{-2}s^{-1}]	log $L_{X,peak}$ [ergs s^{-1}]	log $E_{X,total}$ [ergs]
0123720201	PN	01/05/2000	60.0	37.37±0.61	13.57	30.55	33.17
	RGS		49.9	—	—	—	—
0126130201	PN	07/06/2000	41.9	19.48±0.44	9.72	30.41	32.23
	RGS		58.9	—	—	—	—
0123720301	PN	27/10/2000	55.7	36.76±0.60	4.80	30.10	32.89
	RGS		58.8	—	—	—	—
0133120701	PN	11/12/2000	6.2	15.92±0.39	13.91	30.56	32.71
	RGS		8.8	—	—	—	—
0133120101	PN	11/12/2000	13.4	18.45±0.43	10.41	30.44	33.11
	RGS		60.4	—	—	—	—
0133120201	PN	11/12/2000	4.2	21.81±0.45	8.16	30.33	33.15
	RGS		20.8	—	—	—	—
0134520301	PN	20/01/2001	48.6	35.14±0.59	10.90	30.46	32.58
	RGS		52.2	2.16±	8.71	30.36	33.27
0134520701	PN	22/05/2001	48.2	43.37±0.29	6.83	30.25	32.40
	RGS		49.5	1.55±0.05	6.09	30.20	32.82
0134521301	PN	13/10/2001	—	—	—	—	—
	RGS		39.6	4.54±0.10	15.67	30.61	33.83
0134521501	PN	12/04/2002	15.9	24.58±0.49	8.95	30.37	32.57
	RGS		53.1	3.99±0.12	7.79	30.31	—
0155150101	PN	18/06/2002	4.9	32.46±0.25	11.40	30.47	33.11
	RGS		20.3	3.80±0.12	7.76	30.31	33.32
0134521601	PN	18/06/2002	21.3	34.82±0.26	6.95	30.26	32.09
	RGS		47.8	5.36±0.14	11.29	30.47	—
0134521801	PN	05/11/2002	—	—	—	—	—
	RGS		19.8	5.85±0.15	12.48	30.52	—
0134521701	PN	15/11/2002	—	—	—	—	—
	RGS		19.8	7.02±0.17	15.09	30.60	33.75
0134522001	PN	03/12/2002	—	—	—	—	—
	RGS		22.3	5.43±0.15	11.23	30.47	33.12
0134522101	PN	30/12/2002	—	—	—	—	—
	RGS		48.8	5.50±0.15	10.96	30.46	—
0134522201	PN	23/01/2003	—	—	—	—	—
	RGS		51.8	5.56±0.15	10.96	30.46	—
0134522301	PN	30/03/2003	—	—	—	—	—
	RGS		48.8	3.73±0.12	7.31	30.28	
0134522401	PN	31/05/2003	—	—	—	—	—
	RGS		28.8	4.74±0.14	9.52	30.40	—
0160362701	PN	23/10/2003	—	—	—	—	—
	RGS		26.5	6.61±0.16	13.99	30.57	33.63
0160362801	PN	08/12/2003	—	—	—	—	—
	RGS		53.7	3.86±0.13	7.34	30.29	33.06
0160362901	PN	27/11/2004	—	—	—	—	—
	RGS		56.3	3.93±0.13	8.30	30.34	33.61
0160363001	PN	18/04/2005	—	—	—	—	—
	RGS		52.1	4.23±0.13	8.19	30.33	33.37
0160363201	PN	16/10/2005	—	—	—	—	—
	RGS		50.1	5.02±0.15	10.42	30.44	33.61
0412580101	PN	31/12/2006	—	—	—	—	—
	RGS		44.9	8.14±0.19	17.78	30.67	—
0412580201	PN	19/07/2007	—	—	—	—	—
	RGS		48.8	5.35±0.15	12.44	30.51	33.25
0412580301	PN	03/01/2008	—	—	—	—	—
	RGS		48.8	6.11±0.15	14.45	30.58	33.49
0412580401	PN	04/01/2009	47.0	16.00±1.26	14.02	30.56	32.47
	RGS		48.8	4.60±0.14	10.04	30.42	33.45
0602240201	PN	25/11/2009	57.9	36.93±0.27	10.30	30.43	33.27
	RGS		58.3	4.13±0.13	9.46	30.40	33.30
0412580601	PN	11/01/2010	9.9	14.50±0.38	7.20	30.28	32.99
	RGS		49.8	3.26±0.11	7.38	30.29	30.03
0412580701	PN	02/01/2011	9.9	28.26±0.23	11.15	30.47	33.19
	RGS		62.8	3.16±0.11	6.81	30.25	33.34
0412580801	PN	31/12/2011	9.9	29.80±1.72	11.87	30.49	32.68
	RGS		61.8	2.92±0.11	6.17	30.21	33.26

https://doi.org/10.1017/S1743921316002155 Published online by Cambridge University Press

individual elemental abundances considered are C/H= 0.71 ± 0.10, N/H= 0.90 ± 0.14, O/H= 0.42 ± 0.02, Ne/H= 0.81 ± 0.04, Mg/H= 0.28 ± 0.03, Si/H= 0.25 ± 0.05, S/H= 0.25 ± 0.05, Ar/H= 1.04 ± 0.28, and Fe/H= 0.28 ± 0.01 relative to the solar photospheric values of Grevesse & Sauval (1998).

For flare spectra modelling we used four temperature component, we always include the quiescent emission, i.e. the parameters of the first two temperature components are fixed to the plasma properties of the quiescent emission, whereas, the third and fourth temperature component defines the contribution from the flare. With this approach one accounts for the contribution of the quiescent emission to the overall X-ray emission. Two flare temperature components give a reasonable fit for all bins during the flare decay, this in-turn supports that our assumption of low temperature component is not changing during the flare is correct.

In order to obtain the plasma properties we make use of the total emission measure $EM = \sum_i EM_i$ which is the sum of the emission measures of each temperature component and flare temperature $T = \sum_i \frac{T_i \times EM_i}{EM}$ which is the emission measure weighted sum of the temperatures from each flare component.

3. Results

In Figure 1 (left panel), we plot the distribution of emission measure as a function of flare peak temaperature. The estimated EM from PN and RGS are consistent within the errors. However, we note that the high energy component of the RGS data yields a large error since the instrument is not sensitive at those energies. Hence, it is not meaningful to compare the high temperature component estimated from the RGS with the PN observations.

Solar flares show a remarkable correlation between the temperature and the emission measure (Shimizu *et al.* 1995; Yuda *et al.* 1997]). Stern *et al.* 1992 showed that this correlation can be extrapolated to stellar flares as well. Aschwanden *et al.* (2008) compared the solar and stellar flares. Despite the fact that stellar flare emission are several orders of magnitude higher, the flare peak temperatures and the emission measures follow a common scaling law. In Figure 1 (right panel), we show the comparison of the flare peak temperature and emission measures observed for the Sun, AB Dor, and other stellar flares. Compilation of solar flare as given by Aschwanden *et al.* (2008) are represented as black filled circles. The red and blue squares represent the flares observed on AB Dor by PN and RGS, respectively. Flares observed in other low mass stars compiled by Guedel *et al.* 2004 are depicted as green triangles.

Aschwanden *et al.* (2008) found that the flare peak temperature and emission measure yields a statistical correlation of $EM_f \propto T_f^{4.7\pm0.1}$. This correlation is depicted as purple thick line with 1σ range (purple dashed line). We performed a regression analysis on all the stellar flares and obtained $\mathrm{EM}_f \propto \mathrm{T}_f^{3.2\pm0.3}$. Plotted as black thick line is the scaling law between the flare peak temperature and emission measure obtained from the current analysis. However, we carried out a regression analysis of AB Dor data alone and obtained a slopes of ∼0.39±0.35 for AB Dor flares with correlation co-efficient of 0.17. This very low correlation could be due to the fact that we are dealing with an ultra-fast rotator with a saturated coronae. However, further detailed analysis of a large sample of ultra-fast rotators are to carried out to understand the very small variation in the emission measure during flares.

In Figure (left panel), we plot the total emitted energy in X-rays during a flare as a function of its peak luminosity in 0.2-10 keV energy band. The flare peak X-ray luminosities for AB Dor range from $\sim 10^{30}$ to $\sim 10^{32}$ erg s^{-1} whereas, the flare total X-ray

https://doi.org/10.1017/S1743921316002155 Published online by Cambridge University Press

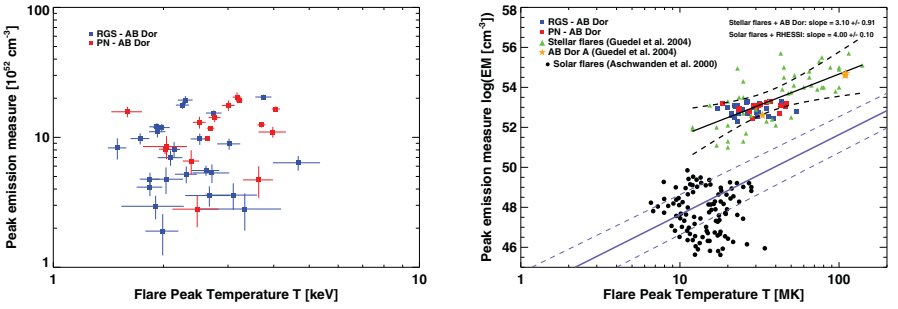

Figure 1. a) Distribution of flare peak emission measure plotted as a function of flare peak temperature for PN (red squares) and RGS (blue squares) data. b) Plot of flare peak emission measure vs. flare peak temperature for the flares observed by *XMM-Newton*. PN and RGS flares are represented by red and blue squares, respectively. Compilation of solar and other stellar flares are depicted black filled circles and green triangles respectively. The linear regression fit with 1σ confidence band to solar flares and stellar flares are depicted as purple and black lines, respectively.

emitted energy ranges from $\sim 10^{32}$ to $\sim 10^{34}$ erg. We note a significant linear correlation between the emitted energy and the luminosity with a correlation co-efficient 0.70. This indicates that the flare duration is essentially independent of amplitude.

Solar micro-flares and milli-flares energies follows a power law (Lin *et al.* 1984; Hudson 1991), $\frac{dN}{dE} = KE^{-\alpha}$, where K is proportionality constant, E is the energy of the flare (ergs) and α is the power law index.

Understanding, if the solar and stellar flare rate distribution steepens at lower energies is very crucial (Hudson *et al.* 1991). For instance, in solar context $\alpha = 1.5 - 1.6$ for a normal flare Crosby *et al.* (1993); whereas $\alpha = 2.3 - 2.6$ for small events in the quiescent corona (Krucker *et al.* 1998). Studies of stellar flare energy distribution in X-rays is rare because of scarcity of stellar flare statistics. Collura *et al.* (1988) found a power-law index $\alpha = 1.6$ for X-ray flares on M dwarfs using EXOSAT observations; on the other hand power-law index $\alpha = 2.2$ for solar analogs EK Dra and 47 Cas was determined by Audard *et al.* (1999). However, it is interesting to know the precise value of α, for example, if the power law is steep then the value $\alpha > 2$, which means that small impulsive events would be sufficient enough to account for the energy output of the entire corona.

Hence the frequency distribution of flare energies, N(E), is a crucial diagnostic to calculate the overall energy residing in flares contained in a given or expected energy range. For each detected flare event on AB Dor, we estimated the energy radiated at X-ray wavelength above quiescent level for both pn and RGS separately. In Fig. 2 (right panel), we plot the frequency distribution of the events as a function of total integrated energy during the flare. Note the slopes for PN and RGS are different since RGS cover more number of energetic flares when compared to PN (1.79 for RGS and 2.04 for PN). Therefore, the large flares may not be contributing to the coronal heating. However, if we extend this distribution below detection threshold we would be able to explain coronal emission by stochastically occurring flares.

4. Summary

We characterised the flares observed on AB Dor observed using *XMM-Newton* over last decade. The resulting flare properties are compared with solare flare properties and we also obtain a common scaling law for the flare peak temperatures and emission measures. Despite the fact that stellar flare emission are ∼250 times higher than solar flares they

https://doi.org/10.1017/S1743921316002155 Published online by Cambridge University Press

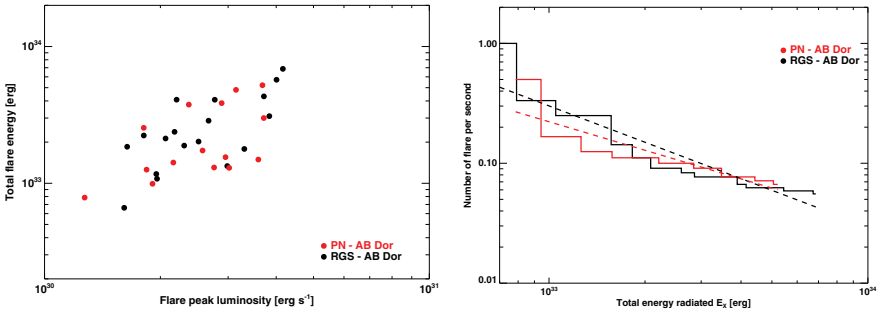

Figure 2. a) Total X-ray emitted energy versus flare peak X-ray luminosity in 0.2-10 keV energy band. Black and red filled circles represent flare observed on AB Dor with RGS and PN, respectively. b) Cumulative frequency distribution of total energy radiated during flare observed with RGS (black) and PN (red). The dashed lines represent the power-law fit to each of the distribution.

follow a common scaling law. Many stellar flares like AB Dor, release an energy of $\sim 10^{34}$ erg, whereas the most energetic solar flares have energies typically around $\sim 10^{32}$ erg. Such high energetic flares observed on AB Dor may suggest a different dynamo action from that of the Sun.

References

Arnaud, K. A. (1996), 'ASP Conf. Ser. 101: Astronomical Data Analysis Software and Systems V', pp. 17–+

Aschwanden, M. J., Stern, R. A. & Güdel, M. (2008), *ApJ* 672, 659–673

Audard, M., Güdel, M. & Guinan, E. F. (1999), *ApJL* 513, L53–L56

Collura, A., Pasquini, L. & Schmitt, J. H. M. M. (1988), *A&A* 205, 197–206

Crosby, N. B., Aschwanden, M. J. & Dennis, B. R. (1993), *Sol. Phys.* 143, 275–299

Grevesse, N. & Sauval, A. J. (1998), *Space sci. rev.* 85, 161–174

Güdel, M. (2004), *A &A rev.* 12, 71–237.

&Guirado, J. C. and Marcaide, J. M. and Martí-Vidal, I. and Le Bouquin, J.-B. and Close, L. M. and Cotton, W. D. and Montalbán, J. 2011, *A&A*, 533, A106

&Henry, T. J. and Subasavage, J. P. and Brown, M. A. and Beaulieu, T. D. and Jao, W.-C. and Hambly, N. C. 2004, *AJ*, 128,2460H

Hudson, H. S. (1991), *Sol. Phys.* 133, 357–369

Lin, R. P., Schwartz, R. A., Kane, S. R., Pelling, R. M. & Hurley, K. C. (1984), *ApJ* 283, 421–425

Krucker, S. & Benz, A. O. (1998), *ApJL* 501, L213

&Kuerster, M. and Schmitt, J. H. M. M. and Cutispoto, G. , 1994, *A&A*, 289, 899K

&Lalitha, S. and Fuhrmeister, B. and Wolter, U. and Schmitt, J. H. M. M. and Engels, D. and Wieringa, M. H. 2013, *A&A*, 560A, 69L

&Lalitha, S. and Schmitt, J. H. M. M. 2013, *A&A*, 559A, 119L

Shimizu, T. 1995, *PASJ*, 47, 251-263

Stern, R. A., Uchida, Y., Tsuneta, S., & Nagase, F. 1992, *ApJ* 400, 321–329 Vilhu & Linsky 1987 Vilhu, O. & Linsky, J. L. 1987, *PASP*, 99, 1071

Yuda, S., Hiei, E., Takahashi, M., & Watanabe, T. 1997, *PASJ*, 49, 115–121

https://doi.org/10.1017/S1743921316002155 Published online by Cambridge University Press